Scientific report
regarding the implementation of the project in the period January-December 2015

Introduction

Transverse momentum spectra of identified charged hadrons in p+p($\bar{p}$) collisions were studied as a function of incident energy below 900 GeV at CERN ISR and SppS and up to 1800 GeV at Fermilab Tevatron colliders. While UA5 Collaboration reported, starting from 200 GeV, an increase of $< p_T >$ of kaons in the central region larger than that expected based on ISR data, the E735 Collaboration evidenced a mass dependent slope of $<p_T>$ as a function of c.m. energy from 300 to 1800 GeV.

Definitely such trend which significantly deviates from a ln(s) extrapolation from lower energies measured at ISR cannot be explained by models based on statistical equilibrium. Detailed studies of E735 Collaboration at 1800 GeV have shown that the increase of $<p_T>$ with dNc/dη depends on the mass of particle.

These studies are of real interest for different QCD inspired models like PYTHIA or EPOS which predict such a dependence as a consequence of a hydrodynamic type evolution with flux tube initial conditions. CDF Collaboration, comparing two energies, i.e. 630 GeV and 1800 GeV, evidenced an energy invariance of the p_T distribution at fixed multiplicity for soft interactions. This shows that the multiplicity of produced particles is a measure of the amount of energy involved in the process. Such a conclusion is supported by recent low relative momentum two-pion correlation studies at 0.9 and 7 TeV which evidenced that the correlation functions at the two energies are similar at a given multiplicity, the size of the emitting system growing with the charged particle multiplicity of the event. It was also evidenced that double and triple partonic interactions start to be significant at higher energies and their cross sections seem to increase linearly with ln(s), where s is the energy in the center of mass of the colliding system.

At about 4 times larger incident energies, as is the case of the present study, such processes contribute to a large energy transfer in the collision volume of proton size which could be well thermalized if we consider the

mean free path of 0.2 – 0.3 fm derived from QGP viscosity and that two – three collisions are in principle sufficient for thermalization.
Therefore is quite probable that at such energies, a piece of matter of proton size, with a radius a few times larger (2.5-4.5) than the mean free path, hydrodynamically explodes if enough energy is produced inside.

In order to evidence such phenomena, a detailed analysis of transverse momentum distributions for high multiplicity and close to azimuthal isotropy events is necessary.
The hadronic final states formed in high energy collisions can manifest different topologies depending on the underlying processes. The topology of each event can be characterized by several event shape variables built using the detected particles. By definition, the event shape observables are designed to measure the energy flow in the collision. They are constructed using both the orientation and the magnitude of each particle momentum. Several event shape observables - ESO - have been used for more than forty years in high energy physics. Originally, these observables were used in jet studies to evidence parton hard scatterings that translate into hadronic jets. The study of jets is a central part of the perturbative QCD studies that extract the properties of quarks and gluons from the hadron distribution in the final event. Using a different approach, in this analysis, event shape observables are used to identify events with random particle distributions. A uniform particle distribution is specific to a non-jetty event. Such isotropic events could reveal properties of the matter created in the collision in the soft region of the spectrum, region described phenomenologically. This approach raises some questions on the event selection performance of the event shape observables. Can events with jets be labeled as uniform by using the event shapes? Is it possible to use the same observables that are used to select jetty events to clean the data sample? Are the selected events in any way biased? Is there a spectrum that randomly distributed in azimuth is not biased by the event shape selection?
Multiplicity is defined as the number of charged particles in a given pseudo-rapidity range. The pseudo-rapidity range used for the multiplicity and the event shape analysis is $|\eta| < 0.8$ in the studies described below.
The event shape observables studied are:
- Directivity – D -measures the normalized momentum deviation from 0 in the positive or negative η ranges [1,2].

- Thrust – T - [3,4] is defined as the normalized maximum value of the momentum projection on an arbitrary axis, summed over all particles in the event.
- Sphericity – S - was introduced in [5] and it measures how close to being spherical the particle distribution in the event is. The spherical shape will be replaced by a circular one when the particles are projected in the transverse plane.
- Recoil – R - measures how well the momentum conservation is reconstructed in the event [6].
- Fox-Wolfram moments – FWM – were introduced by G.C. Fox and S. Wolfram in [7].

Charged particles [8]

A detailed study, already reported, of the multiplicity dependence of the efficiency has been done first. The multiplicity bins for global and combined multiplicity are presented in Table 1. The combined multiplicity is of special interest as the efficiency proves to be independent of the multiplicity.

Trigger	Estimator / Bin no.	Global	Combined	Mean Combined Multiplicity
Minimum Bias	0	0-5	0-6	3.26
	1	6-9	7-12	9.17
	2	10-14	13-19	15.59
	3	15-22	20-28	23.25
	4	23-31	29-39	32.72
	5	32-39	40-49	43.31
	6	40-49	50-59	53.21
High Multiplicity	1	40-49	50-59	53.21
	2	50-62	60-71	63.57
	3	63-72	72-82	75.27
	4	>72	>82	87.63

Table 1

Efficiency studies – event shape dependence

Particles reconstructed in analyzed events do not always originate in the primary vertex. The most probable sources of contamination are particle decays and secondaries produced in the particle interaction with the material present in the experiment. Also, some particles will not be detected due to the limited acceptance and efficiency or the interaction with the material. Both effects can be evaluated using Monte Carlo simulations once

the detector response and the material distribution in the experiment are known. Therefore, the efficiency dependence on the event shape cuts was also studied. Tracking efficiency for event shape selection in each multiplicity bin is plotted in Figures 1, 2, 3 and 4. The first row contains the first three bins, followed by the last three minimum bias bins on the second row. For Sphericity, Thrust and Directivity, the efficiency is plotted in red, green and blue corresponding to the low, medium and high values for each of the event shapes. The medium values are defined as the values between the isotropic and non-isotropic regions. For the Fox-Wolfram moments, red is used for the azimuthally isotropic events, while green is for everything else. For all the event shape observables, the efficiency at low transverse momenta is higher for ”isotropic” events and lower at high p_T values. Events with low p_T particles are preferentially selected by the event shape observables. Either these events have a non-biased efficiency that would allow the event to be selected as uniform, or events containing higher p_T particles must have a low efficiency in that p_T region in order to lose those particles. A bias towards low transverse momenta can be achieved if the efficiency at high p_T is low and the particles with low p_T are well reconstructed. The argument can be mirrored for the ”non-isotropic” events where the low momenta contribution is reduced by a low efficiency and the high momenta must have a high reconstruction probability. The bias is smaller for high multiplicity bins.

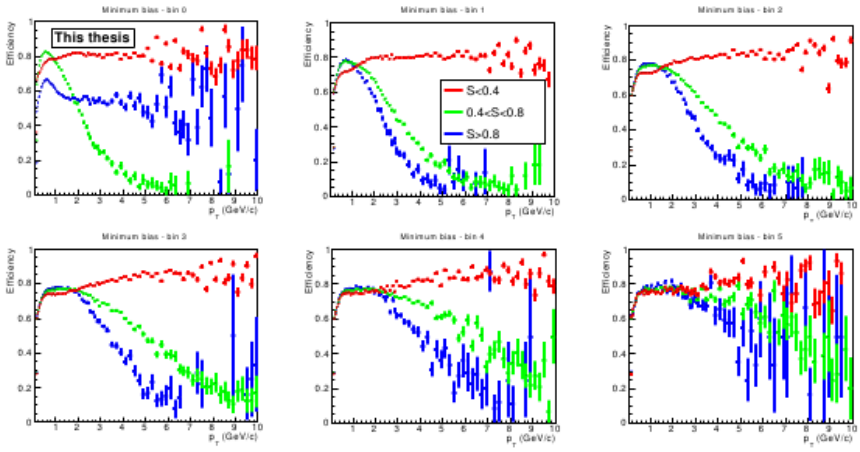

Figure 1: Efficiency in multiplicity bins for sphericity event selection. Isotropic events (S > 0.8) are plotted in blue. Green correspond to events with sphericity between 0.4 and 0.8. The efficiency for the pencil-like events with S < 0.4 is plotted in red.

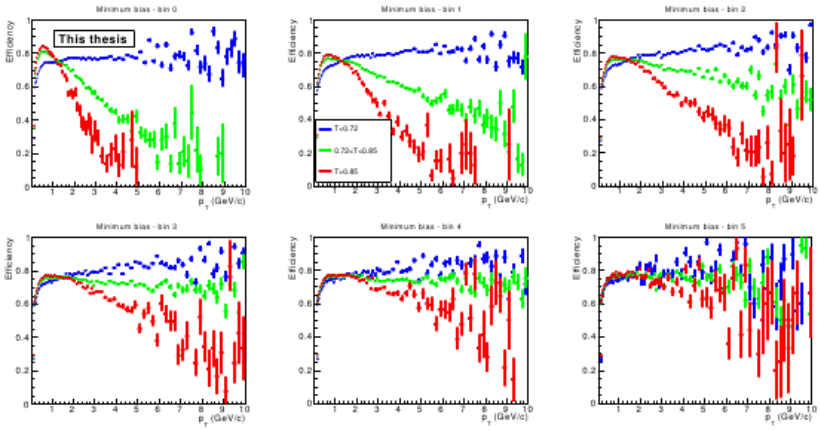

Figure 2: Efficiency in multiplicity bins for thrust cuts. Isotropic events (T < 0.72) are plotted in blue. Green correspond to events with thrust between 0.72 and 0.85. The efficiency for the pencil-like events with T > 0.85 is plotted in red.

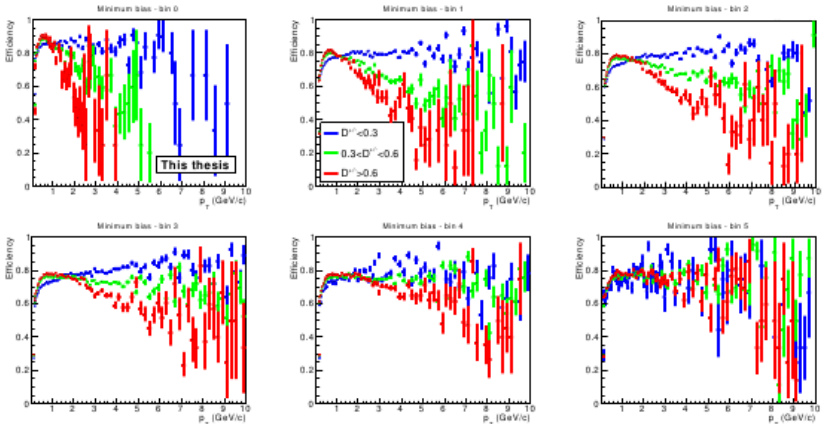

Figure 3: Efficiency in multiplicity bins for directivity cuts. The efficiency for isotropic events is plotted in red, the pencil-like events in blue, and events with medium directivity values in green.

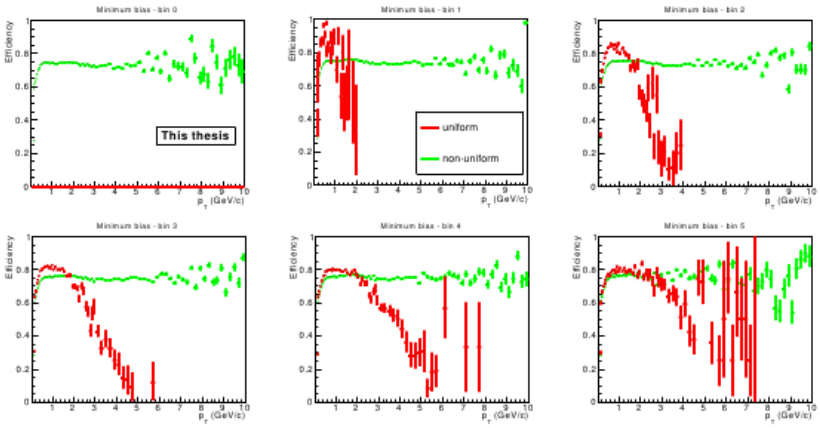

Figure 4: Efficiency for multiplicity bins using Fox-Wolfram cuts. In red, the azimuthally isotropic events are plotted. The efficiency for the rest of the events is plotted in green.

Event shape selected spectra

For all the multiplicity bins the event shape cuts were applied. The transverse momentum spectra for event shape cuts in all the multiplicity bins are presented. The efficiency correction was done bin wise using the efficiencies from Figures 1,2,3,4. The feed-down correction used was the one from minimum bias, the same as for the minimum bias multiplicity spectra. For the minimum bias multiplicity bins, the results for sphericity, directivity, thrust and Fox-Wolfram cuts are plotted in Figures 5,6,7,8. The multiplicity bins are displayed as follows: the first three bins are plotted in order on the first row and the last three bin on the second row. All the spectra are normalized to the number of events analyzed in the corresponding class. For all the event shape cuts, the spectra for “non-isotropic” events have long tails. The events labeled as “isotropic” have a “softer” shape.

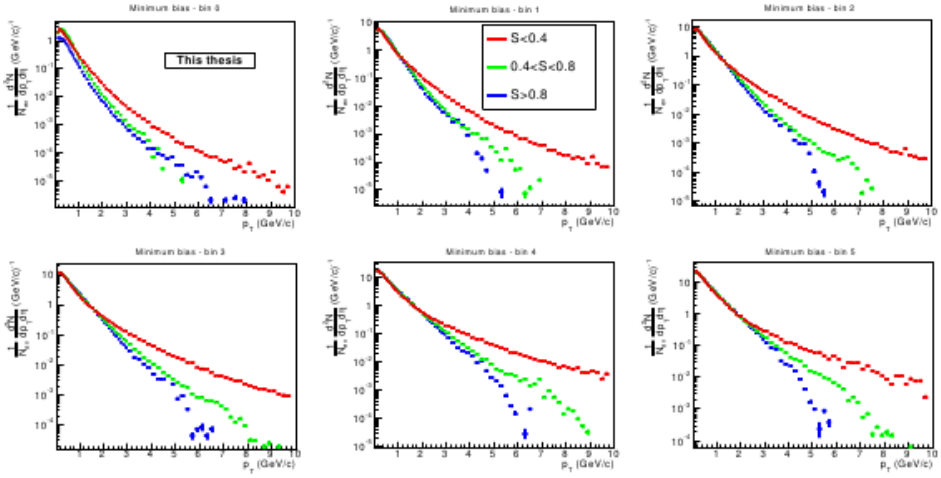

Figure 5: Transverse momentum spectra in six minimum bias bins and three sphericity cuts.

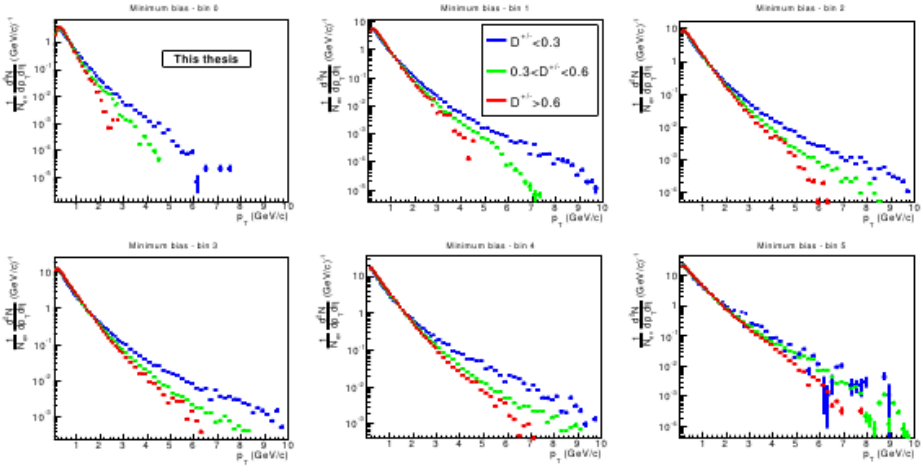

Figure 6: Transverse momentum spectra in six minimum bias bins and three directivity cuts.

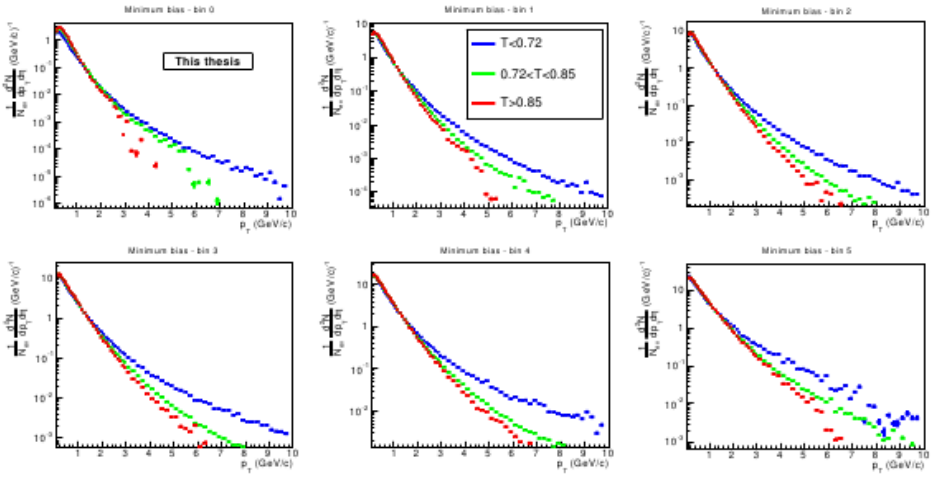

Figure 7: Transverse momentum spectra in six minimum bias bins and three thrust cuts.

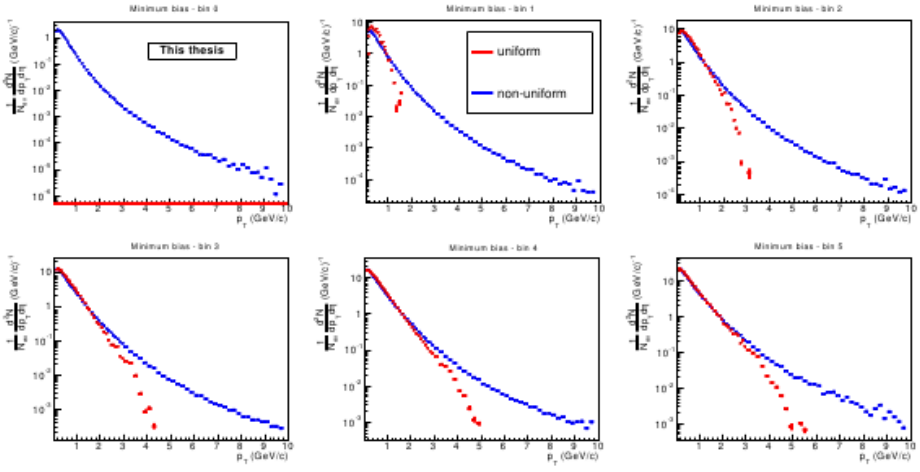

Figure 8: Transverse momentum spectra in six minimum bias bins and Fox-Wolfram moments cuts corresponding to isotropic and non-isotropic events.

The spectra for events close to azimuthal isotropy, selected with the sphericity, thrust, directivity and Fox-Wolfram moments are plotted in Figures 9 and 10. The slope of the transverse momentum distributions for the events selected in this way, is changing with the multiplicity. The power law tails observed in the p_T spectra for different multiplicity bins are drastically reduced in Figures 9 and 10 where nearly azimuthal isotropic events were selected.

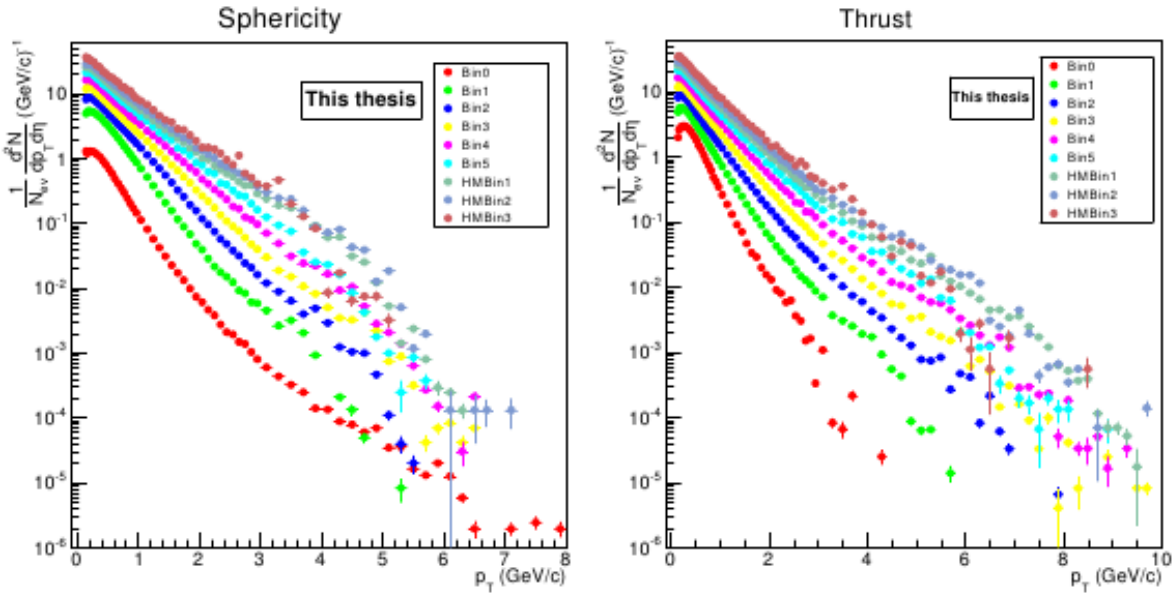

Figure 9: Transverse momentum spectra for minimum bias and high multiplicity events in multiplicity bins and sphericity (left panel) and thrust (right panel) selection for uniform events.

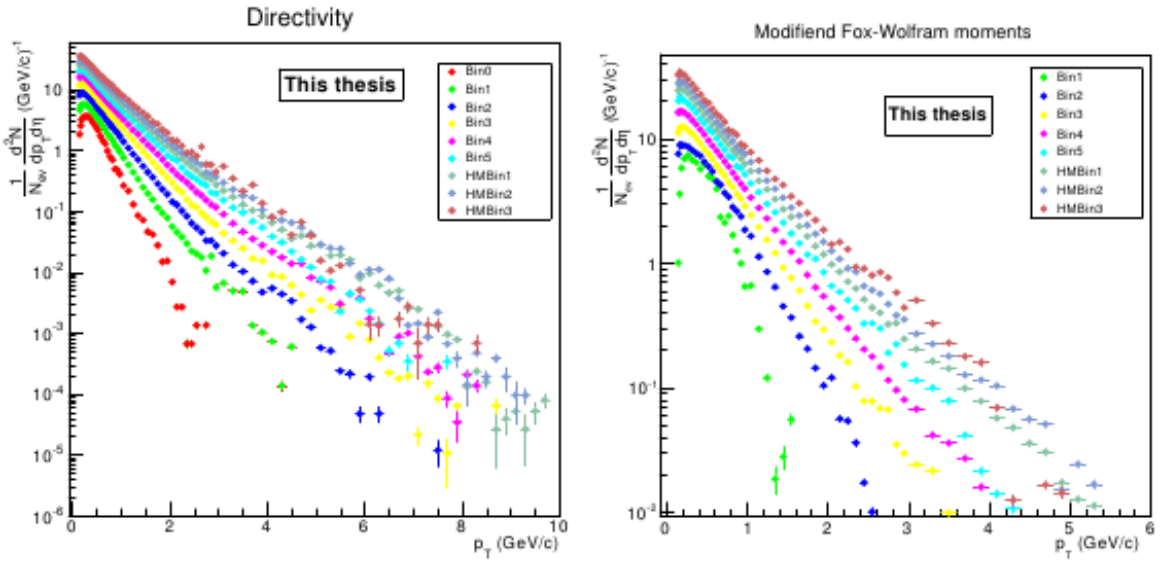

Figure 10: Transverse momentum spectra for minimum bias and high multiplicity events in multiplicity bins and directivity (left panel) and Fox-Wolfram moments (right panel) event selection for uniform events.

Identified charged hadrons [9,10]

Events with high azimuthal isotropy are of a special interest for this analysis. In order to estimate the degree of azimuthal isotropy the global observable directivity was used. The events with a high azimuthal isotropy will

have a low directivity. For events dominated by jets the directivity increases towards 1.
The two dimensional directivity (computed as the mean of D^+ and D^-) versus multiplicity representation is shown in Fig. 11.

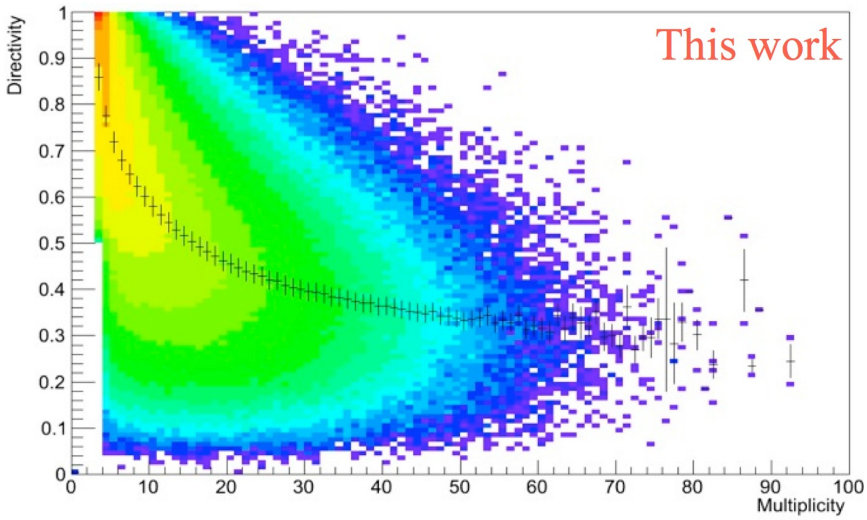

Figure 11: Two dimensional directivity (mean of D^+ and D^-) versus combined multiplicity.
A $d^2N/\Delta\varphi\Delta\eta$ two dimensional representation for minimum bias and multiplicity >30 & directivity <0.3, where $\Delta\varphi$ and $\Delta\eta$ represent the difference in pseudo-rapidity and azimuthal angle between a given identified charged hadron and the leading particle in the respective event, can be used in order to evaluate the performance of the estimation (Fig. 12 and 13).

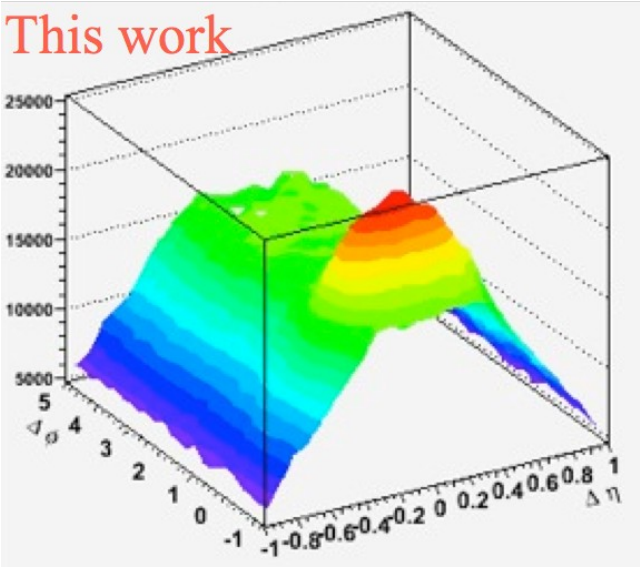

Figure 12: Two dimensional $d^2N/\Delta\varphi\Delta\eta$ representation for the minimum bias case.

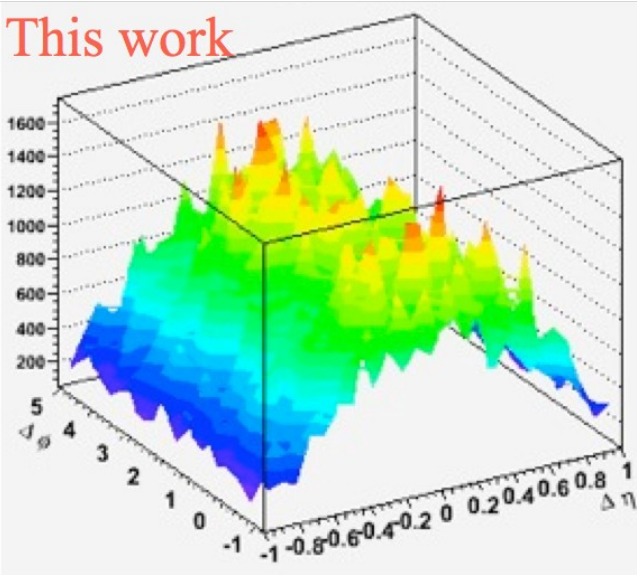

Figure 13: Two dimensional $d^2N/\Delta\varphi\Delta\eta$ representation for M>30 & D<0.3.

Even without extracting the background correlation one could observe, comparing the two distributions, that high multiplicity and low directivity cut removes the jet-like correlation observed in the minimum bias case [10].

In the case of the selections using the events multiplicity based on the combined multiplicity estimator, there is no dependence of the corrections as a function of multiplicity. When on top of the multiplicity selection an extra cut using the event directivity is applied this is no longer the case. For the low multiplicity bins the corrections show a strong variation with the directivity of the considered events. However, as the multiplicity increases this dependence becomes smaller very fast. For a combined multiplicity above 40 this variation is below 3%. Consequently, as in the case of the spectra in multiplicity bins, the MB determined corrections were used also for the spectra in directivity bins, only for events with multiplicity above 40. The mentioned 3% variation for the tracking, matching, PID efficiency and percentage of misidentified particles was included in the systematic errors. For this analysis three directivity ranges were established: directivity lower then 0.3, 0.3 to 0.6 and 0.6 to 0.9. In order to consider an event to be in one of the above mentioned directivity classes both D^+ and D^- have to fulfill simultaneously the imposed condition. A visual representation of the selected events in terms of mean directivity and combined multiplicity is shown in Fig. 14, where only events for which the simultaneous D^+ and D^- condition was fulfilled. This procedure selects samples with high purity but it decreases considerably the available statistics.

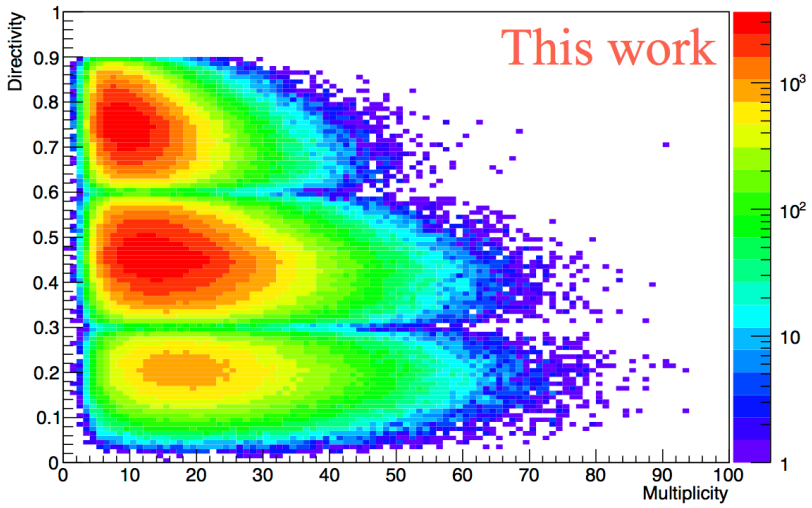

Figure 14: Two dimensional directivity (mean) versus combined multiplicity - filled only when simultaneous D^+ and D^- condition was fulfilled.

In Fig. 15 the p_T spectra for the highest four multiplicity bins and the three directivity classes are plotted. As it can be seen, for the high directivity class the available statistics is very low. The statistical errors, total systematic errors and the systematic errors related with the multiplicity and directivity selections are plotted separately as in the case of the p_T spectra as a function of multiplicity.

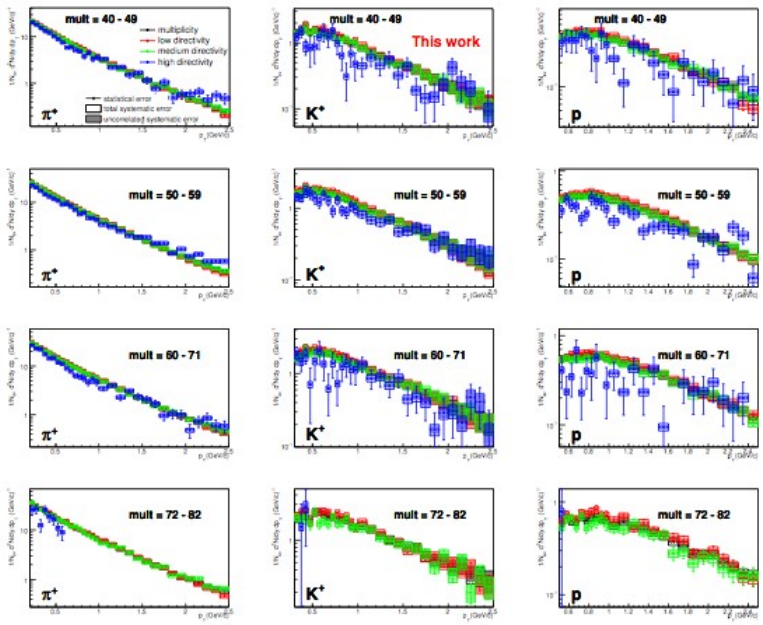

Figure 15: p_T spectra as a function of directivity in the highest four multiplicity bins

The change of the shape of the p_T spectra can be easier followed in Fig. 16 where the ratio of the spectra of all the three directivity classes to the spectra in the respective multiplicity bin is plotted.

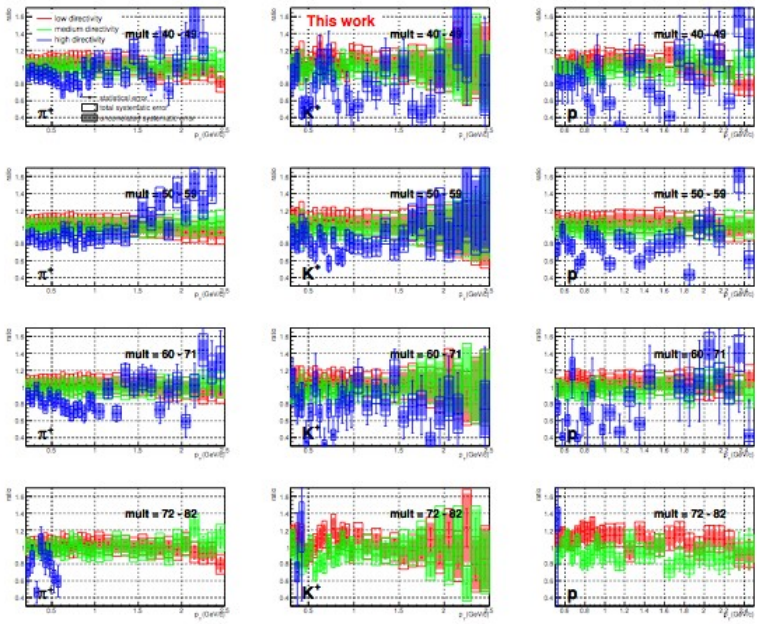

Figure 16: ratio of the p_T spectra as a function of directivity relative to the spectra in the corresponding multiplicity bin.

In low directivity events (red symbols) an enhancement of the low p_T region and a depletion of the high p_T can be observed, relative to the corresponding multiplicity selected spectra. For the high directivity events (blue symbols) the behavior of the spectra mirrors the one for the low directivity events, being much harder. As expected, spectra obtained by using the medium directivity selection (green symbols) is very similar with the spectra in the corresponding multiplicity bins.
For the multiplicity bin 50 - 59 where the statistical fluctuations are reasonably low, the three directivity classes were plotted separately (Fig. 17). In this representation it can be seen that the crossing point between the enhancement at low p_T and the depletion at high p_T (for the low directivity bin) moves towards a higher p_T value with the increase of the mass of the considered particle, being around 1.6 GeV/c for pions and above 2.2 GeV/c for protons. The behavior of the p_T spectra in the three directivity classes as a function of multiplicity is shown in Fig. 18. A clear change in the spectra shapes for all three species is evidenced going from large directivity values

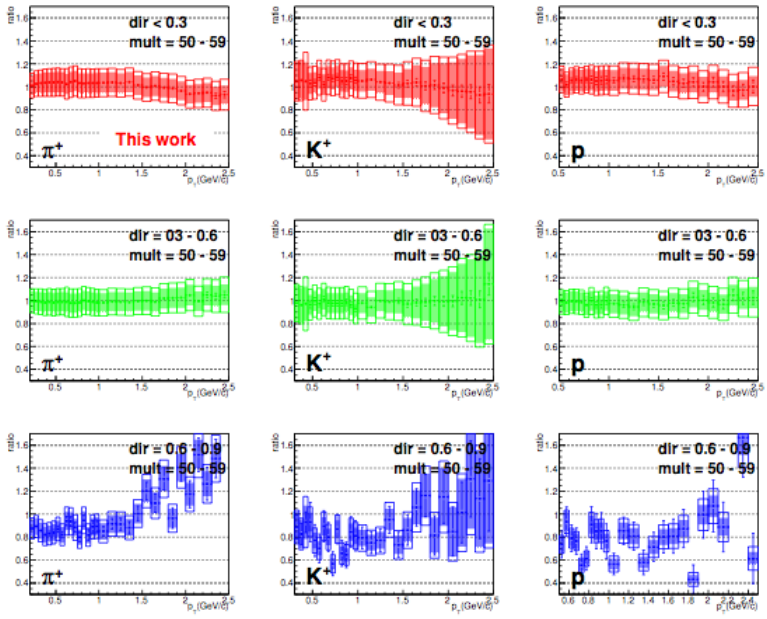

Figure 17: ratio of the p_T spectra as a function of directivity in the 50 - 59 multiplicity bin, plotted separately.

towards low values specific for less jetty events.

While for pions the change is from exponential plus power law shape to exponential one, for kaons and protons a transition from exponential shape to a concave one with maxima at $\sim$ 0.6 GeV/c and 0.8 – 0.9 GeV/c, respectively, is observed.

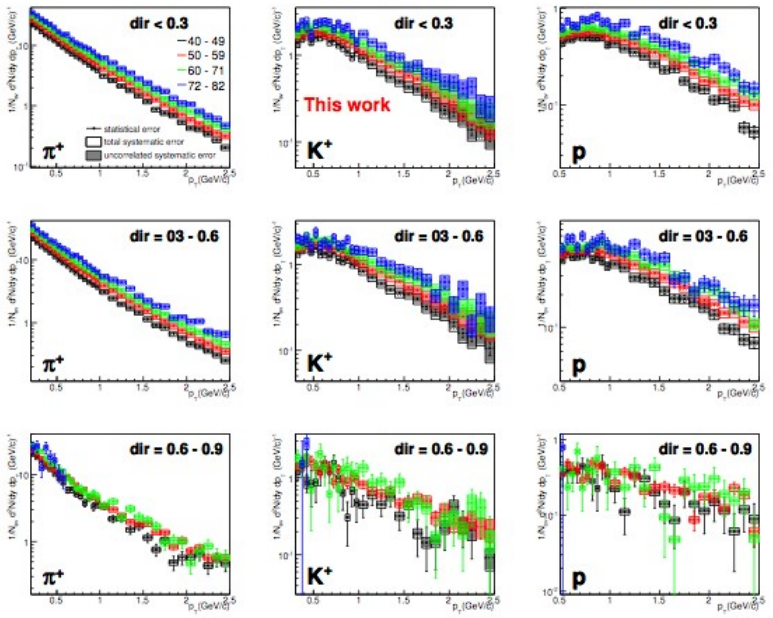

Figure 18: p_T spectra as a function of multiplicity in all the three directivity classes.

<pT> and yields

The studies of event shape selection of events have been then postponed as in the meantime further studies regarding the multiplicity selector dependence have been started. Similar to heavier systems, the studies based on the forward detector V0M amplitude selection were triggered by the necessity to minimize the autocorrelation effects, if they manifest, and compare systems on the same basis. Charged particle and identified hadron spectra have been obtained in different percentiles and in Figs. 19, 20, 21 below are shown the ones for pions, kaons and protons. For this V0M selector the range in p_T for PID data analysis has been significantly enlarged by combining several analyses on different transverse momentum ranges.

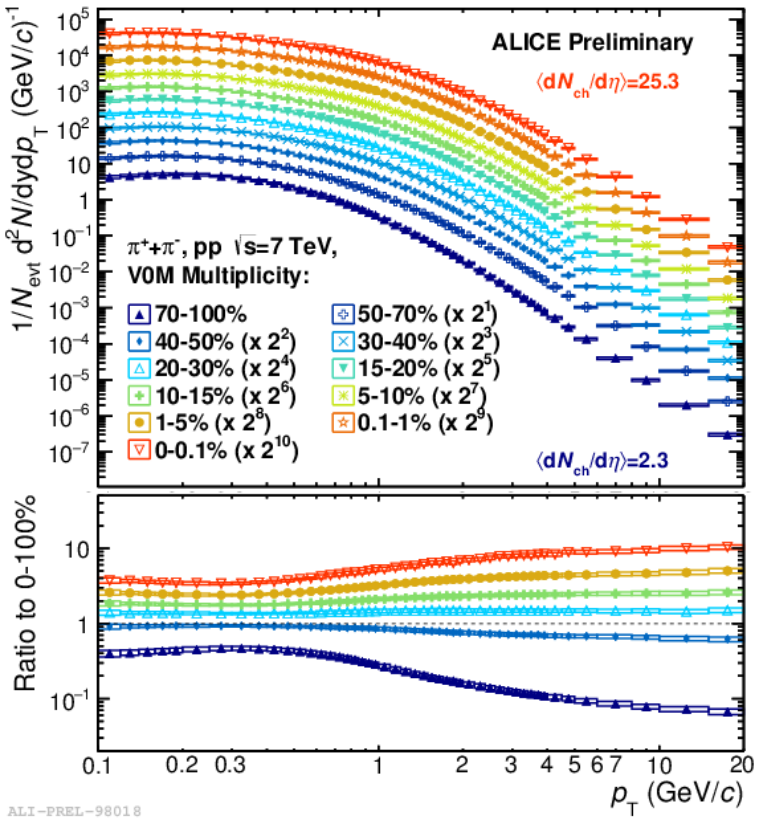

Figure 19: Pion spectra in V0M percentile bins, pp collisions at 7 TeV

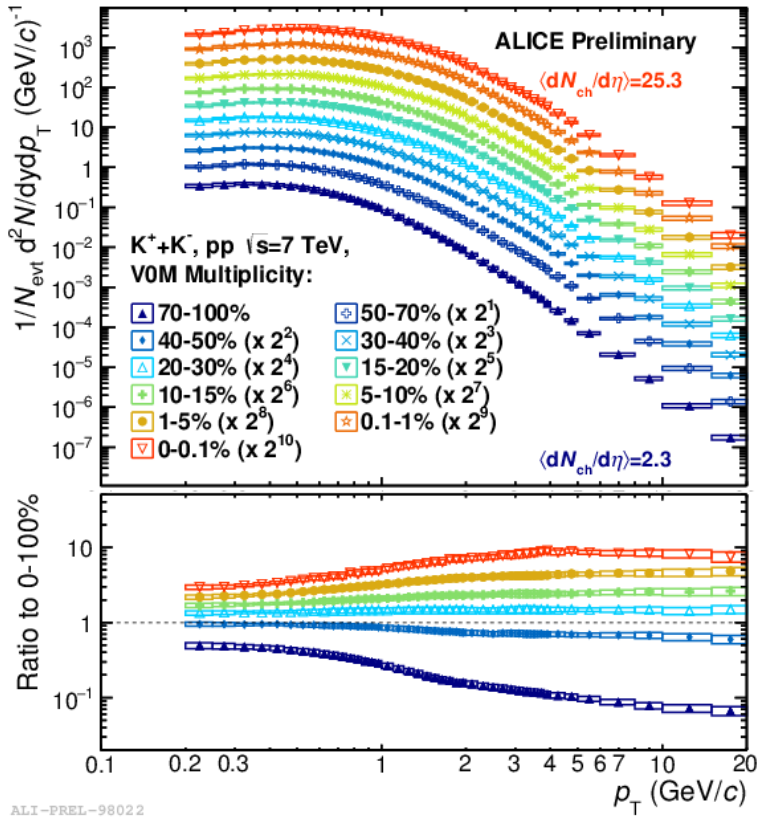

Figure 20: Kaon spectra in V0M percentile bins, pp collisions at 7 TeV

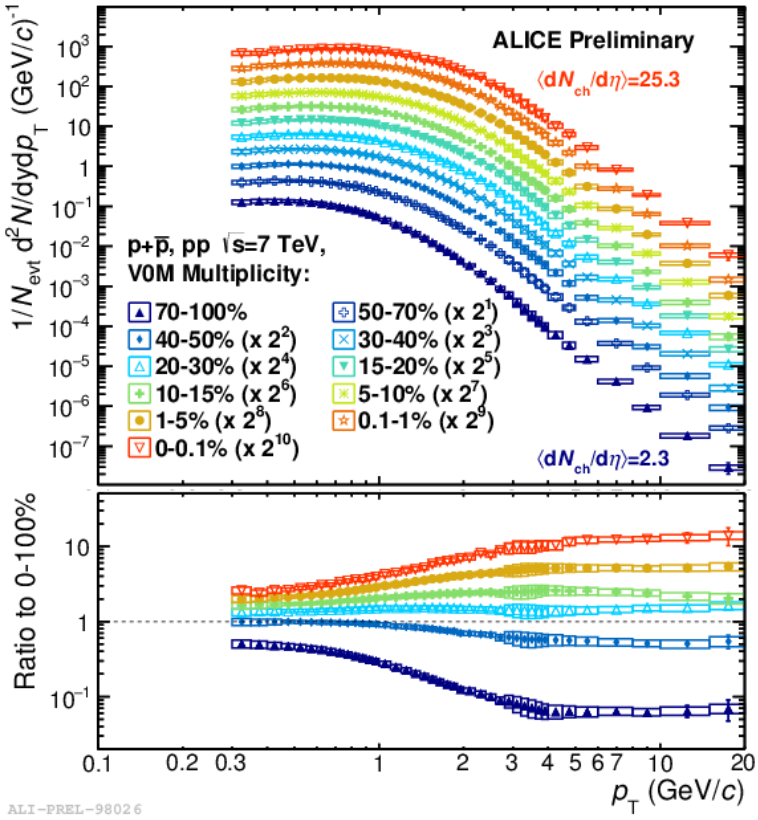

Figure 21: Proton spectra in V0M percentile bins, pp collisions at 7 TeV

Starting from these large transverse momentum range spectra the average transverse momentum and yields have been extracted using different fit functions. The fit quality for different fit functions is shown in Figs. 22 and 23. The functions are named 1 to 3 from left to right in Fig. 22 and 4 and 5 from left to right in Fig. 23.

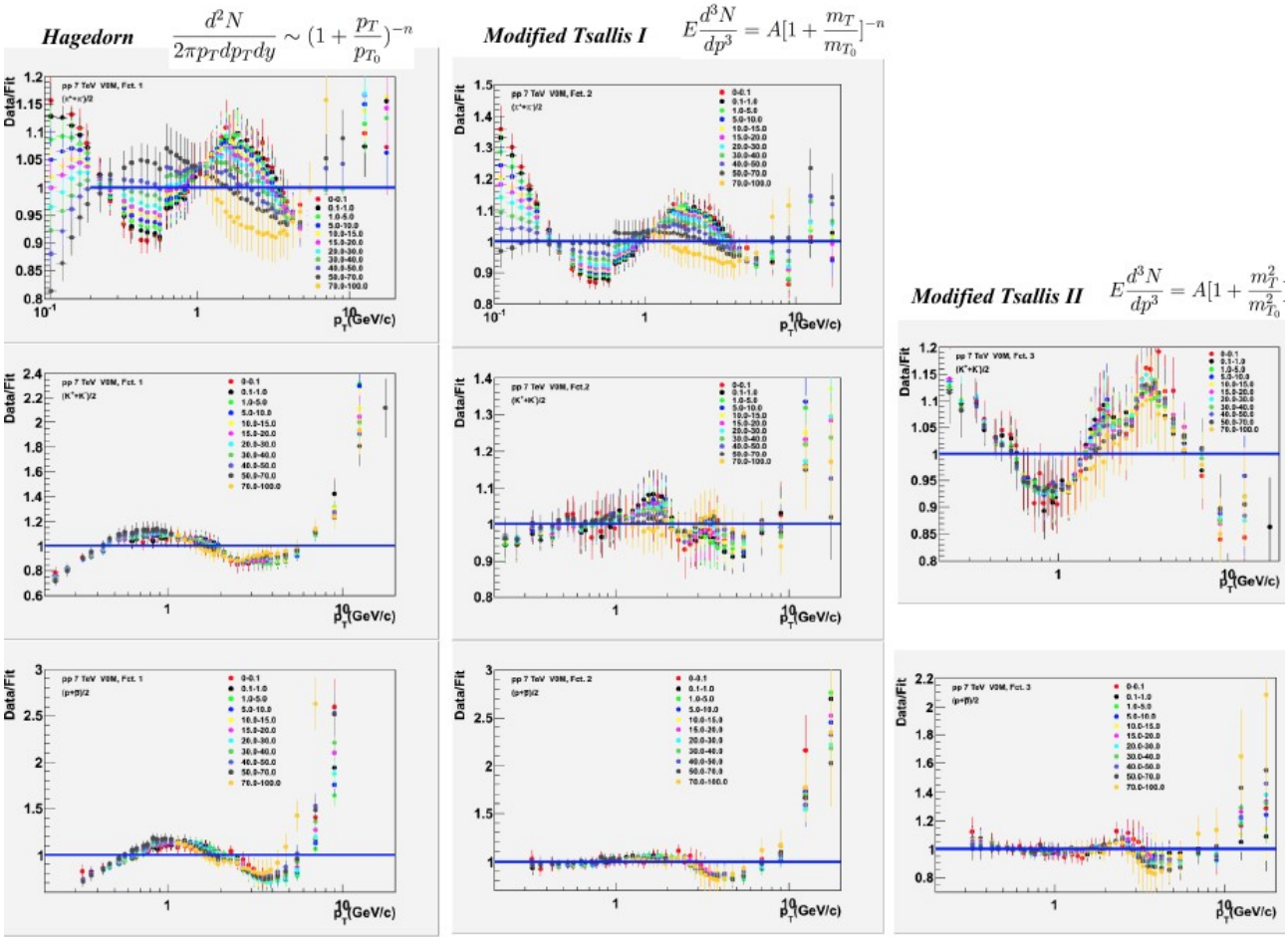

Figure 22: Fit quality

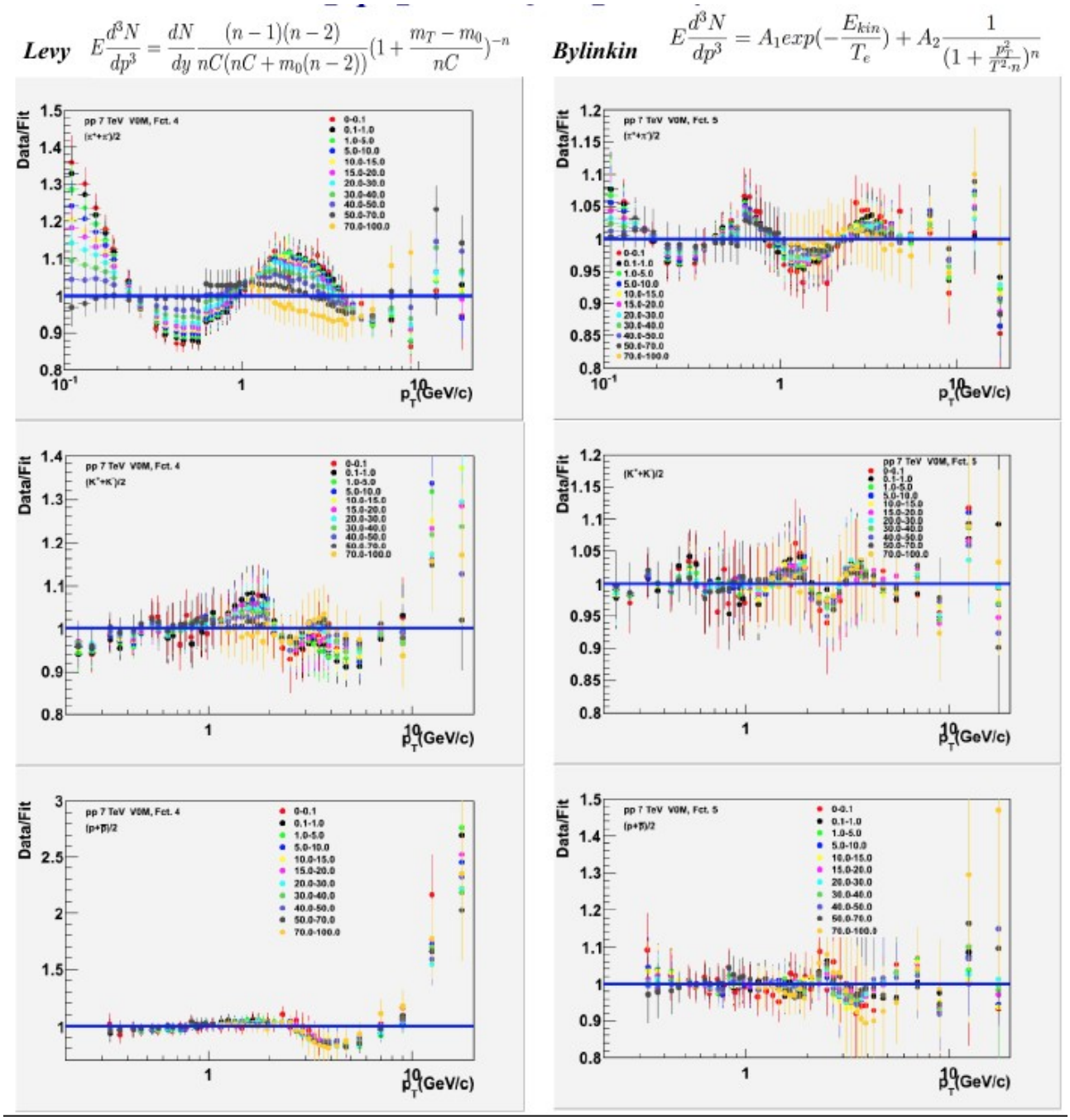

Figure 23: Fit quality

The fit quality for function 5 (Bylinkin) is the best one (in the limit of 5% variation of the data to fit ratio).

The results for <p_T> and yield ratios are shown in Figs. 24 and 25 for the different fit functions.

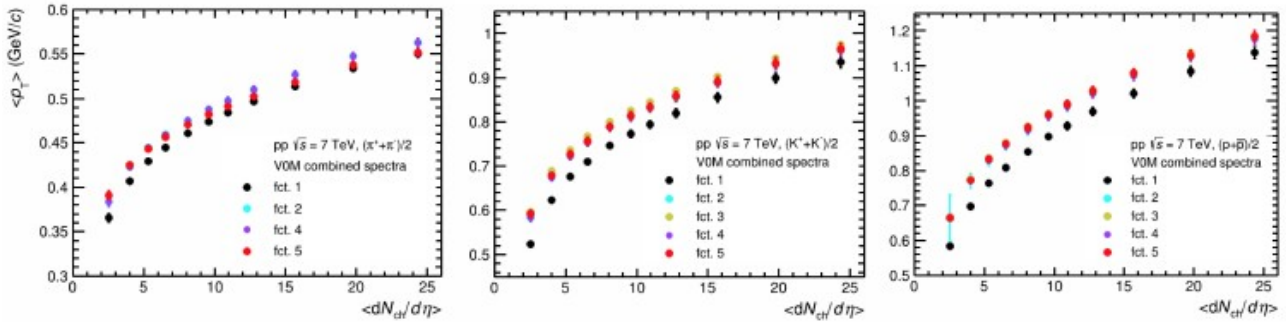

Figure 24: <p_T> for pions, kaons and protons as a function of the average charged particle multiplicity with different fit functions.

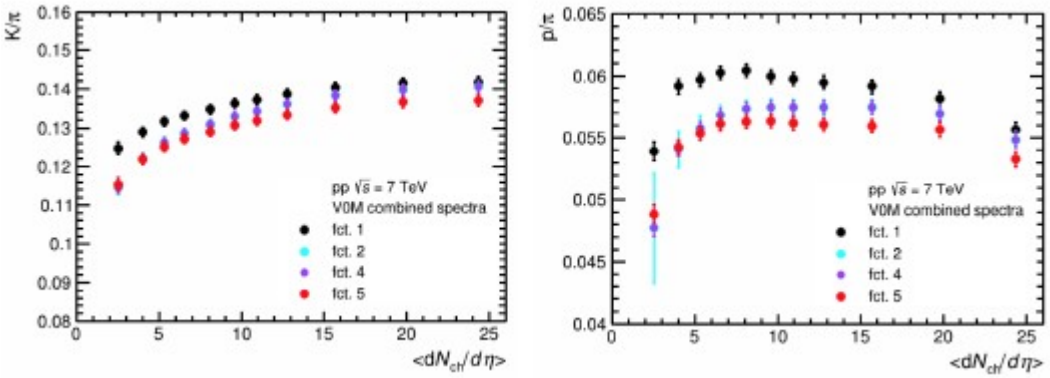

Figure 25: K/π and p/π yield ratios as a function of the average charged particle multiplicity with different fit functions.
The difference between the best fit function results and the others can be used to esimate the systematic error due to the fit.

Conclusions

The possibility to select highly isotropic events in pp collisions at 7 TeV has been studied on the experimental data. The shapes of the obtained spectra in different multiplicity & event shape selections clearly depend on the selection variable and its value. By combining several detectors extended spectra in the average transverse momentum have been obtained for different multiplicity estimators for charged particles and identified hadrons. Based on these several fit formulas of the spectra have been used in order to obtain the average transverse momentum and yield ratios. This analysis is quite robust now. More statistics and further checks on the

efficiency corrections are needed in order to draw firm conclusions on the behaviour of the similar observables selected also with different event shape variables.

Study of Non-Perturbative Particle Production in Strong Colour Fields. Collective Effects and Their Dependence on Multiplicity at LHC energies

Effects of strong longitudinal colour electric fields (SCF), on the production of particles in nucleus-nucleus (Pb + Pb), proton-nucleus (p + Pb) and proton-proton (p + p) collisions were studied based on HIJING model and especially the new version (v2.0) of the HIJING/$B\bar{B}$ developed by us to simulate heavy ion collisions at ultra-relativistic energies.
Here we focus our analysis at two energies of interest: $\sqrt{s}$= 0.9 TeV and $\sqrt{s}$= 7 TeV, where data for charged particles and identified particles (ID) have been reported for MB events. The model calculations including SLCF effects give a good description of the spectral shape at low p_T (p_T <4 GeV/c) for both energies. At high p_T (p_T > 5 GeV/c) the calculatinos lead to a somewhat harder spectrum than that observed.
In our phenomenology this could indicate that jet quenching, i.e., suppression of high p_T particles like that observed at RHIC energies in nucleus-nucleus collisions, could also appear in p+p collisions, particularly for events with large multiplicity [11].
Figure 26 compares the ALICE results to the predicted mid-rapidity spectra for positive pions (solid histograms), kaons (dashed histograms), and protons (dotted histograms) in minimum bias p+p collisions.
There is agreement in the p_T region of interest $1 < p_T < 4$ GeV/c at both energies. The over-prediction for proton and kaon production below p_T = 1 GeV/c is consistent with possible presence of radial flow, which seems to be larger at 7 TeV than at 0.9 TeV.
The radial flow could appear as a consequence of a hydrodynamic type evolution with flux tube initial conditions [12], not embedded in our model.

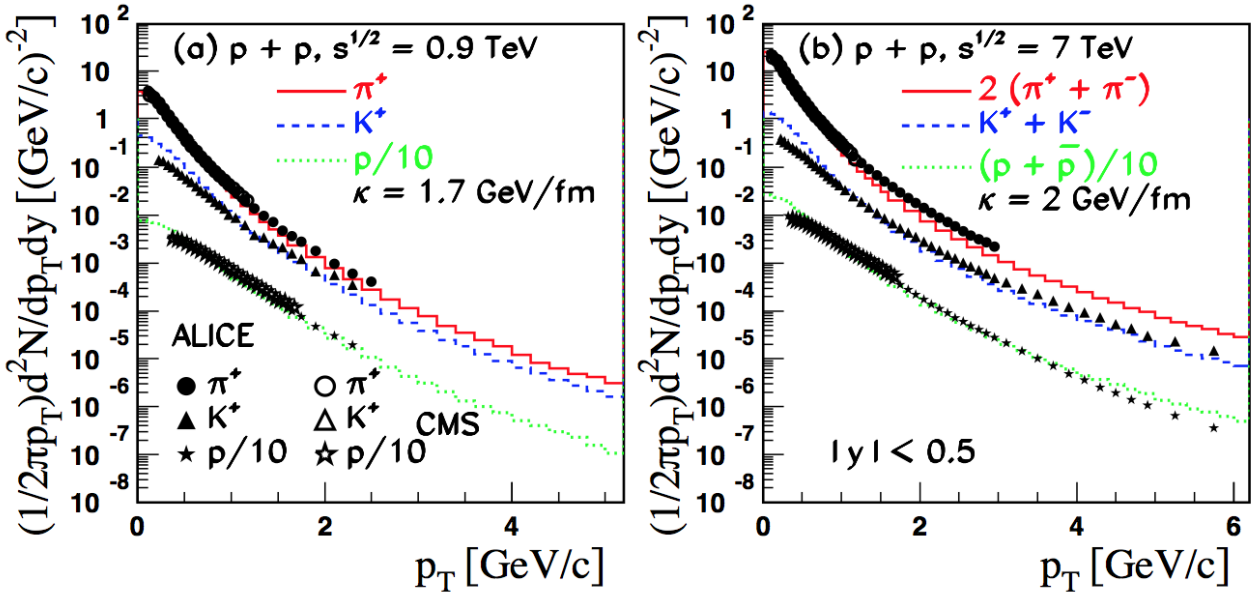

Figure 26: HIJING/ $B\bar{B}$ v2.0 predictions of transverse momentum spectra at mid- rapidity (|y| < 0.5) for mesons (π,K) and baryons (p) at √s = 0.9 TeV (left panel) and at √s = 7 TeV (right panel) are compared to data. The data (closed symbols) are from ALICE [13]. Data (open symbols) are from CMS collaboration [14] and are plotted using a normalization factor 0.78, since the data are measured in a different rapidity interval. Statistical error bars on the data points are smaller than the markers.

We extend our analysis to the production of (multi)strange baryons. In Fig. 27 we show the HIJING/$B\bar{B}$ v2.0 model predictions of p_T spectra at mid-rapidity (|y| < 0.5) for Λ (solid histograms), Ξ^- (dashed histograms) and Ω^- (dotted his tograms) baryons at 0.9 TeV and 7 TeV. For (multi)strange particles, the data indicate a stronger radial flow at 7 TeV than at 0.9 TeV. For the p_T region of interest, 1 < pT < 4 GeV/c, the model results are in agreement with data at both energies.

The ALICE Collaboration has reported measurements of the transverse momen tum distribution of prompt open charmed mesons (D^0, D^+ , D^{*+} , $D_S{}^+$) in p + p collisions at √s= 7 TeV [15, 16], and of (D^0, D^+, D^{*+}) at √s = 2.76 TeV [17] in the central rapidity range |y| ≤ 0.5. Prompt indicates D mesons produced at the p + p interaction point, either directly in the hadronization of the charm quark or in strong decay of excited charm resonances. The contribution from weak decays of beauty mesons, which give rise to feed-down D mesons, were subtracted. The model calculations include SCF effects [18]. The energy dependence of string tension $\kappa(s) = \kappa_0\ (s/s_0\ )^{0.04}$ GeV/fm, predict a modest increase when going from √s = 2.76 TeV (κ = 1.88 GeV/fm) to √s = 7 TeV

(κ = 2.03 GeV/fm). Therefore, to calculate prompt open charmed mesons production we consider the same value of average string tension for charm and strange quark, i.e, $\kappa_C = \kappa_S \approx 2$ GeV/fm. The theoretical results are compared to data in Fig. 28. Predictions for D_S^+ mesons at $\sqrt{s}$ =2.76 TeV are also included. The agreement between theory and experiment is good within experimental uncertainties, except at $\sqrt{s}$ = 7 TeV where while the average cross section is well reproduced the predicted spectrum has a somewhat shallower slope than the data.

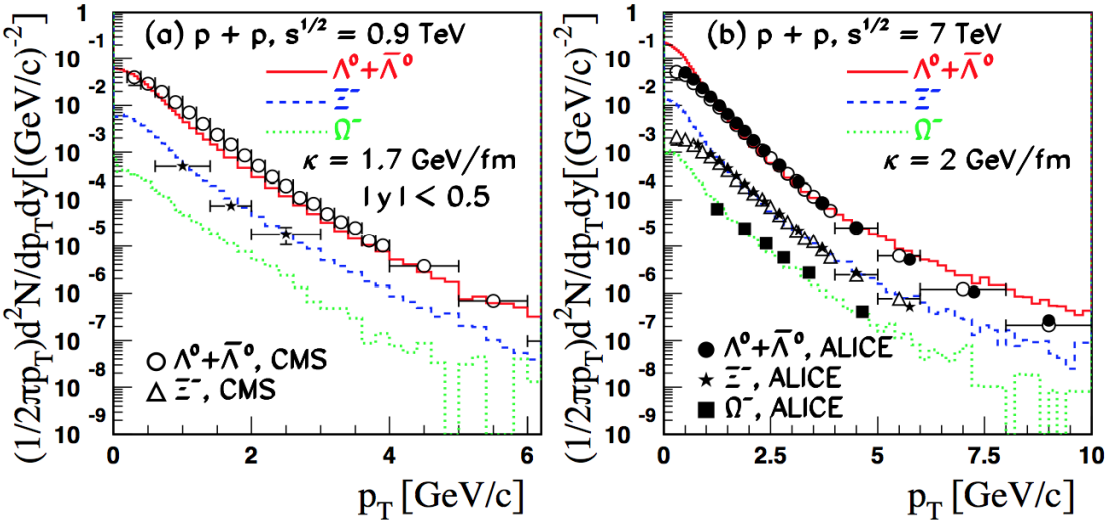

Figure 27: HIJING/B$\bar{B}$ v2.0 predictions of transverse momentum spectra at mid-rapidity (|y| < 0.5) for (multi)strange hyperons (Λ, Ξ, Ω) at $\sqrt{s}$= 0.9 TeV (left panel) and at$\sqrt{s}$ = 7 TeV (right panel) are compared to data. The data are from the ALICE [19,20] (closed symbols) and CMS collaborations [21](open symbols). Error bars include only the statistical uncertainties.

The average transverse momenta as function of charged particle multiplicity ($<p_T>(N_{ch})$) are shown in Fig. 29 for pp collisions at $\sqrt{s}$ = 7 TeV in comparison with ALICE data. It seems that mean charged particle as global observable is not a sensitive observable for SCF effects, and the data are well described with $\kappa = \kappa_0 = 1$ GeV/fm.

The $< p_T > (N_{ch})$ of identifed particles (ID), i.e. $\pi^+ + \pi^-$, $K^+ + K^-$, ($p + \bar{p}$, $\Lambda + \bar{\Lambda}$, $\Xi^+ + \Xi^-$, $\Omega^- + \Omega^+$) are shown in Fig. 30. The average transverse momentum of ID particle is more sensitive to the collective expansion. A model calculation for $< p_T >$ as function of multiplicity for various hadron species show that the change in the shape of the value of $< pT >$ due to the transverse expansion is dependent on the individual hadron species of different mass. While the protons gain most in $< p_T >$, the pions lose some $< p_T >$.

Therefore, the protons experience large flow-effect and could not be described

by our model calculations.

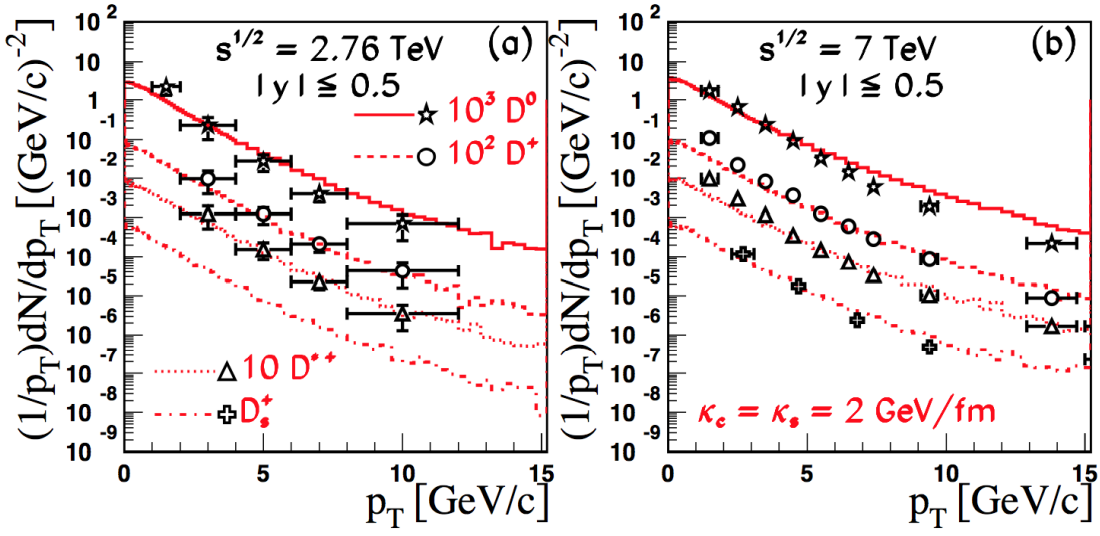

Figure 28: HIJING/$B\bar{B}$ v2.0 predictions for p_T distributions at mid-rapidity for p+p → (D + $\bar{D}$)/2 + X with D = D^0 (solid histograms); D = D^+ (dashed histogram); D = D^{*+} (dotted histograms); and D = D_s^+ (dash-dotted histogram). The results are compared to data at √s = 2.76 TeV (left panel) from Ref. [17] and at √s = 7 TeV (right panel) from Refs. [15,16]. For clarity, the experimental data and theoretical results are multiplied with a factor indicated in the figure. Only statistical error bars are shown.

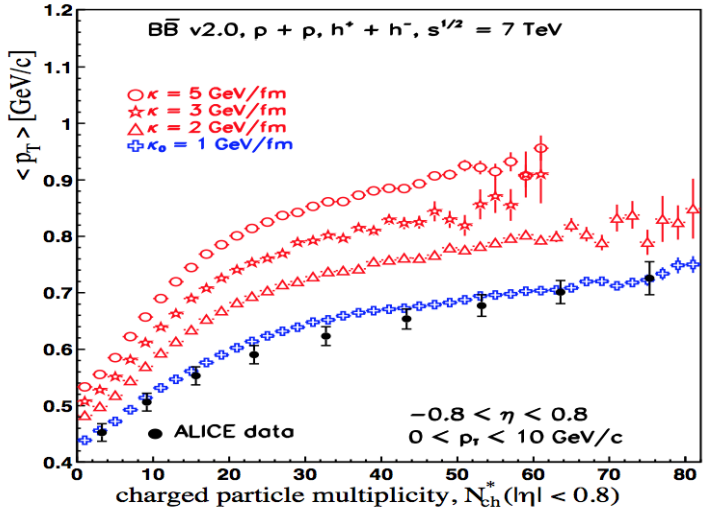

Figure 29: The HIJING/$B\bar{B}$ v2.0 model predictions for average transverse momentum < p_T > as a function of number of charged-particle multiplicity (N_{ch}) in pp collision at √s = 7 TeV. The data are from ALICE [22] . The error are systematic uncertainties on < p_T >. The statistical errors are negligible.

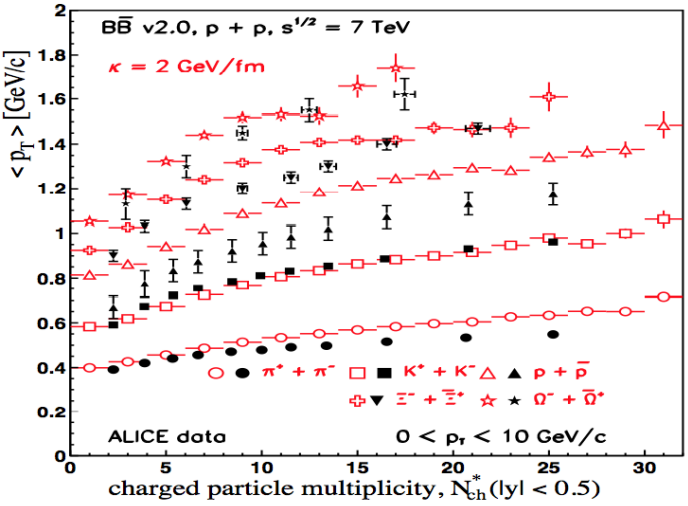

Figure 30: The HIJING/BB̄ v2.0 model predictions for average transverse momentum $< p_T >$ of ID particles as a function of number of charged-particle multiplicity (N_{ch}) in pp collision at $\sqrt{s}$ = 7 TeV. The data are from ALICE [22] . The error are systematic uncertainties on $< p_T >$ The statistical errors are negligible.

Figure 31 present the model predictions of $< p_T >$ (Nch) for p + Pb collisions at 5.02 TeV. The calculations include SCF effects and JJ̄ loops. The model predict a mass hierarchy and this fact could be quantitatively understood in hydrodynamics. For ID particles the $< p_T >$ in p + Pb collisions at $\sqrt{s_{NN}}$ = 5.02 TeV increases with multiplicity, at a rate which is stronger for heavier particles.

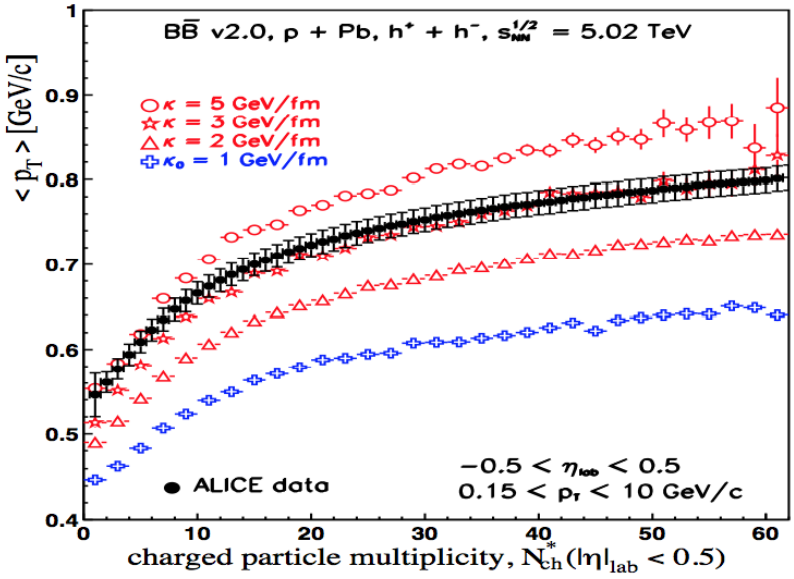

Figure 31: The HIJING/BB̄ v2.0 model predictions of mean transverse momentum as function of charged particle multiplicity for p + Pb collisons at $\sqrt{s_{NN}}$ = 5.02 TeV. The data are from ALICE [22]. The errors are systematical uncertainties.

References

[1] P. Beckmann et al., Collective Azimuthal Alignment in Relativistic Heavy Ion Reactions, Mod. Phys. Lett. A 2, 163 (1987)

[2] J. P. Alard and the FOPI Collaboration, Midrapidity source of intermediate-mass fragments in highly central collisions of Au + Au at 150A MeV, Phys. Rev. Lett. 69 (1992) 889.

[3] S. Brandt, Ch. Peyrou, R. Sosnowski and A. Wroblewski, The principal axis of jets – an attempt to analyse high-energy collisions as two-body processes, Phys. Lett. 12 (1964) 57

[4] E. Fahri, Phys. Quantum Chromodynamics Test for Jets, Rev. Lett. 39 (1977) 1587

[5] J.D. Bjorken and S.J. Brodsky, Statistical Model for Electron-Positron Annihilation into Hadrons, Phys. Rev. D1 (1970) 1416

[6] A. Banfi, Resummed event shapes at hadron-hadron colliders, JHEP 0408 (2004) 062, arXiv:hep-ph/0407287v3

[7] G.C. Fox and S. Wolfram, Event shapes in e+ e– annihilation, Nucl. Phys. B149 (1979) 413.

[8] A. Herghelegiu, PhD Thesis, University of Bucharest

[9] C. Andrei, PhD Thesis, University of Bucharest

[10] Cristian Andrei, Ionela Berceanu, Alexandru Bercuci, Andrei Herghelegiu, Francesco Noferini, Mihai Petrovici, and Amalia Pop. Transverse momentum distributions of pions, kaons an pro- tons for high multiplicity and close to azimuthal isotropic events in 7 tev pp collisions with the alice experiment at the lhc (short analysis note based on the previous notes and presentations). Inter- nal Note, April 2012. https://twiki.cern.ch/twiki/pub/ALICE/ PWGLFPAGSPECTRAMultiplicityEventShapePP7/coll_ph_pp_ALICE_ internal_note_310111.pdf. 91

[11] Abelev B et al (ALICE Collaboration), Phys. Rev. Lett. 110 032301 (2013)

[12] K. Werner, I. Karpenko, T. Pierog, M. Bleicher and K. Mikhailov, Phys. Rev. C 83, 044915 (2011)

[13] M. Chojnacki (ALICE Collaboration), J. Phys. G 38, 124074 (2011)

[14] V. Khachatryan et al. (CMS Collaboration), CMS PAS FSQ-12-014 (2012)

[15] B. Abelev et al. [ALICE Collaboration], JHEP 1201, 128 (2012)

[16] B. Abelev et al. [ALICE Collaboration], Phys. Lett. B 718, 279 (2012)
[17] B. Abelev et al. [ALICE Collaboration], JHEP 1207, 191 (2012)
[18]V. T. Pop, M. Gyulassy, J. Barrette, C. Gale and M. Petrovici,
J. Phys. G 41, 115101 (2014)
[19] B. Abelev et al. (ALICE Collaboration), Phys. Lett. B 712, 309 (2012)
[20] K. Aamodt et al. (ALICE Collaboration), Eur. Phys. J. C 71, 1594 (2011)
[21] V. Khachatryan et al. (CMS Collaboration), JHEP 1105, 064 (2011)
[22] B. B. Abelev et al. [ALICE Collaboration], Phys. Lett. B 727, 371 (2013)

Project Manager,

Prof. Dr. Mihai Petrovici